Preprints of the 21st IFAC World Congress (Virtual)
Berlin, Germany, July 12-17, 2020

Gap Opening Controller Design to Accommodate Merges in Cooperative Autonomous Platoons ⋆

Wouter J. Scholte * **Peter W.A. Zegelaar** *,** **Henk Nijmeijer** *

* *Mechanical Engineering Department, Eindhoven University of Technology, Eindhoven, Netherlands (e-mail: w.j.scholte@tue.nl, p.zegelaar@tue.nl, h.nijmeijer@tue.nl).*
** *Ford Motor Company, Research and Advanced Engineering Europe, Aachen, Germany (e-mail: pzegelaa@ford.com)*

Abstract: In this paper, a cooperative platoon-based gap opening controller is developed. The intended application is gap creation in cooperative platoons to accommodate merges with spatial restrictions. Therefore, the main objective is to execute the maneuver in a predefined time. The controller design is based on a regular cooperative adaptive cruise control algorithm with an additional feedforward term for a desired gap. Experimental validation of the controller is performed with small mobile robots. The proposed control strategy is capable of opening the gap in a predefined time. In future work, this strategy can be used in the design of a merging algorithm specifically for CACC platoons.

Keywords: Autonomous vehicles, Automotive control, Closed-loop gain, PD controllers, Trajectory planning

1. INTRODUCTION

Connected automated vehicles (CAV) can play an important role in tackling some current transportation challenges. For example, CAVs may reduce fuel consumption, emissions, and traffic congestion by using cooperative adaptive cruise control (CACC) (Rios-Torres and Malikopoulos (2016)). Vehicles utilizing CACC can drive closely together in a string while communicating their control input. Such a string of vehicles is often referred to as a platoon. The advantage of communication is that vehicles can drive closer together while *string stability* is maintained. *String stability* is a notion describing the mitigation of disturbances down the string. If disturbances dampen, the platoon is said to be string stable. Without this property, longitudinal disturbances of the leader vehicle cause larger excitations at the back of the string.

Loss of string stability may be caused by communication delays between the vehicles. String stability despite these delays can be achieved by using a velocity-dependent inter-vehicle distance. In essence, the desired inter-vehicle distance is a *headway time* multiplied by the vehicle's velocity. A constant *stand still distance* may be added, which essentially is a coordinate transformation and does not effect the dynamics. Experimental results using this control strategy have been presented in Ploeg et al. (2011). Due to the proven practical capabilities, this controller will be the basis of the controller design in this paper.

⋆ This work is part of the research program i-CAVE with project number 14893, which is partly financed by the Netherlands Organisation for Scientific Research (NWO).

For practical implementation of CACC, the platoon formation needs to be controlled. Adding a new vehicle to the platoon while driving has been a topic of interest in recent research. An overview of the current research can be found in the survey of Rios-Torres and Malikopoulos (2016). Platooning-specific techniques are discussed but are not the main focus of this survey. The examples of platooning in the survey do not employ a velocity-dependent inter-vehicle distance. However, two platoons utilizing a velocity-dependent inter-vehicle distance were merged during the Grand Cooperative Driving Challenge (GCDC). The platoons employed a heuristic control strategy in which the vehicles linearly switch their target vehicle (Hult et al. (2018)). At the end of this maneuver all vehicles thus drove at a correct distance from their new preceding vehicle. However, during this alignment the following of the desired trajectory cannot be guaranteed. This may affect the timely opening alignment of the vehicles.

This paper focuses on the gap creation in a platoon as it is a fundamental part of the merging maneuver. Previous research regarding gap creation often focused on the desired longitudinal trajectory rather than the vehicle control (Ntousakis et al. (2016), Wang et al. (2017)). However, to accommodate scenarios with spatial constraints, such as highway on-ramps, a timely execution of the maneuver is required. Therefore, a longitudinal controller is designed. The proposed controller maintains the benefits of a regular CACC controller while opening the gap in a timely fashion. The controller was experimentally validated using small robots. The vehicle model and controller designs are discussed in Section 2, which is concluded with simulations. Section 3 elaborates on the design of the experiments and shows their results. The paper is concluded in Section 4.

2. CONTROL STRATEGY

The proposed control strategy is based on the vehicle model and controller of Ploeg et al. (2011). This strategy can be used for regular CACC driving and varying the inter-vehicle distance. The vehicle model and controller design are both discussed in this section. Furthermore, the controller is analyzed and simulations are performed.

2.1 CACC and Inter-vehicle Distance Control

The longitudinal dynamics of each vehicle is described using

$$\dot{q}_i(t) = v_i(t) \tag{1}$$
$$\dot{v}_i(t) = a_i(t) \tag{2}$$
$$\dot{a}_i(t) = \frac{1}{\tau}u_i(t) - \frac{1}{\tau}a_i(t). \tag{3}$$

Where q_i, v_i and a_i are the 1-D position, velocity and acceleration of the i^{th} vehicle. The control input is denoted with u_i and the driveline dynamics are represented using time constant τ. It is assumed that τ is equal for all vehicles.

An example of a platoon is shown in Figure 1 which consists of vehicle i and $i-1$. The distance between the front bumper of vehicle i and the rear bumper of vehicle $i-1$ is denoted with d_i. The vehicles are equipped with radar therefore vehicle i can measure d_i and its derivative $\dot{d}_i = v_{i-1} - v_i$. Wireless communication allows for data transfer between the vehicles.

A controller aims to keep the vehicle at a desired inter-vehicle distance

$$d_{r,i}(t) = hv_i(t) + r + \gamma(t). \tag{4}$$

Where h and r denote the headway time and the stand still distance. The purpose of r is to maintain a safe distance at low velocities. The additional gap is denoted with γ, which is zero during normal driving. The error is defined as $e_i = d_i - d_{r,i}$, with the corresponding error states $[e_{1,i}\ e_{2,i}\ e_{3,i}] = [e_i\ \dot{e}_i\ \ddot{e}_i]$. This yields the error dynamics

$$e_{1,i} = d_i - d_{r,i} \tag{5}$$
$$e_{2,i} = v_{i-1} - v_i - \dot{\gamma} - ha_i \tag{6}$$
$$e_{3,i} = a_{i-1} - a_i\left(1 - \frac{h}{\tau}\right) - \ddot{\gamma} - \frac{h}{\tau}u_i \tag{7}$$
$$\dot{e}_{3,i} = -\frac{1}{\tau}e_{3,i} + \frac{1}{\tau}u_{i-1} - \frac{1}{\tau}\xi_i, \tag{8}$$

where

$$\xi_i = h\dot{u}_i + u_i + \ddot{\gamma} + \tau\dddot{\gamma}. \tag{9}$$

Based on (8) a function of ξ is designed that controls the error dynamics and compensates for u_{i-1}, such that

$$\xi_i = [k_\mathrm{p}\ k_\mathrm{d}]\begin{bmatrix}e_{1,i}\\ e_{2,i}\end{bmatrix} + u_{i-1}. \tag{10}$$

Where scalars k_p and k_d are control parameters. Now (9) and (10) yield the control law

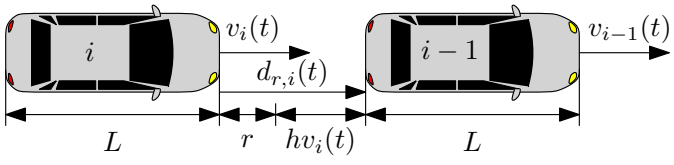

Fig. 1. Definition of the platoon during steady state driving.

$$\dot{u}_i = \frac{1}{h}\left([k_\mathrm{p}\ k_\mathrm{d}]\begin{bmatrix}e_{1,i}\\ e_{2,i}\end{bmatrix} + u_{i-1} - u_i - \ddot{\gamma} - \tau\dddot{\gamma}\right). \tag{11}$$

This control law can be used for gap opening. However, the designed trajectory of gap distance γ must have C^2 continuity such that $\dddot{\gamma}$ can be obtained at all times.

The stability of the individual vehicle's error dynamics is investigated. These dynamics are investigated by writing them in the form

$$\begin{bmatrix}\dot{e}_{1,i}\\ \dot{e}_{2,i}\\ \dot{e}_{3,i}\\ \dot{u}_i\end{bmatrix} = \begin{bmatrix}0 & 1 & 0 & 0\\ 0 & 0 & 1 & 0\\ \frac{-k_p}{\tau} & \frac{-k_d}{\tau} & -\frac{1}{\tau} & 0\\ \frac{k_p}{h} & \frac{k_d}{h} & 0 & -\frac{1}{h}\end{bmatrix}\begin{bmatrix}e_{1,i}\\ e_{2,i}\\ e_{3,i}\\ u_i\end{bmatrix} + \begin{bmatrix}0 & 0\\ 0 & 0\\ 0 & 0\\ \frac{1}{h} & \frac{-1}{h}\end{bmatrix}\begin{bmatrix}u_{i-1}\\ \ddot{\gamma} + \tau\dddot{\gamma}\end{bmatrix}. \tag{12}$$

This system has an equilibrium in the origin for $u_i = 0$ and $\ddot{\gamma} + \tau\dddot{\gamma} = 0$. Similar to Ploeg et al. (2011) the Routh-Hurwitz stability criterion can be applied to the state matrix. It follows that the error dynamics are stabilized for $h > 0$ and any $k_p > 0$ and $k_d > 0$ that satisfy $k_d > k_p\tau$.

2.2 Controller Analysis

The proposed controller is compared to two feedback control strategies, which do not consider $\ddot{\gamma}$ and $\dddot{\gamma}$ in the computation of u_i. The feedback controllers differ in their computation error $e_{2,i}$. One controller uses the derivative $\dot{\gamma}$ in the error computation. The other assumes γ constant and computes $e_{2,i}$ by only using measurements $v_{i-1} - v_i$ and a_i. The three controllers are referred to as *feedforward controller*, *feedback controller assuming a differentiable* γ, and *feedback controller assuming a constant* γ respectively. They will be discussed separately in this section.

Feedforward controller (FF) The feedforward controller is designed in the previous section. It is subject to control law (11) and requires a γ-trajectory with C^2 continuity. To isolate the influence of the gap opening maneuver, it is assumed that the preceding vehicle is driving at a constant velocity v_{nom}. In essence, $v_{i-1} = v_{nom}$, $a_{i-1} = 0$, and $u_{i-1} = 0$. Now define states x and outputs y as

$$x = [e_i,\ v_i - v_{i-1},\ a_i,\ u_i,\ \dot{\gamma},\ \ddot{\gamma}]^T \tag{13}$$
$$y = [e_i,\ v_i - v_{i-1},\ a_i]^T, \tag{14}$$

the system can be written in the form

$$\dot{x} = \begin{bmatrix}0 & -1 & -h & 0 & -1 & 0\\ 0 & 0 & 1 & 0 & 0 & 0\\ 0 & 0 & -\frac{1}{\tau} & \frac{1}{\tau} & 0 & 0\\ \frac{k_p}{h} & -\frac{k_d}{h} & -k_d & -\frac{1}{h} & -\frac{k_d}{h} & -\frac{1}{h}\\ 0 & 0 & 0 & 0 & 0 & 1\\ 0 & 0 & 0 & 0 & 0 & 0\end{bmatrix}x + \begin{bmatrix}0\\ 0\\ 0\\ -\frac{\tau}{h}\\ 0\\ 1\end{bmatrix}\dddot{\gamma} \tag{15}$$

$$y = \begin{bmatrix}1 & 0 & 0 & 0 & 0 & 0\\ 0 & 1 & 0 & 0 & 0 & 0\\ 0 & 0 & 1 & 0 & 0 & 0\end{bmatrix}x. \tag{16}$$

Using this linear time invariant model, the system can be analyzed in frequency domain. First, the frequency domain transfer function between the requested γ and error e_i is investigated. The influence of γ rather than input $\dddot{\gamma}$ is examined because the units of γ and e_i are both meters. The relation is described using transfer function

$$\frac{e_i(s)}{\gamma(s)} = s^3 \frac{e_i(s)}{\dddot{\gamma}(s)} = 0. \tag{17}$$

It can thus be concluded that e_i is not influenced by changing γ if this control law is used if the initial conditions are all zero. Therefore, the vehicle will maintain the requested inter-vehicle distance for any C^2 continuous γ-trajectory without creating an error.

The inter-vehicle distance (d_i) of the vehicle in relation to the desired gap γ is another performance indicator. This shows the longitudinal behavior for changes in γ. It can be noted that $\frac{d_i(s)}{\gamma(s)} = \frac{-v_i(s)}{\dot{\gamma}(s)} = \frac{-a_i(s)}{\ddot{\gamma}(s)}$. The response in distance is thus strongly related to the response in velocity and acceleration. These responses can be obtained using input $\dddot{\gamma}$ and output v_i or a_i with the formulas $\frac{d_i(s)}{\gamma(s)} = -s^2 \frac{v_i(s)}{\dddot{\gamma}(s)} = -s \frac{a_i(s)}{\dddot{\gamma}(s)}$. This yields transfer function

$$G_{FF}(s) = \frac{d_i(s)}{\gamma(s)} = \frac{1}{1+hs}. \tag{18}$$

The transfer functions can be seen as a low-pass filter. Since $h > 0$ the maximum gain of the functions is 1. In other words, the high frequency excitations of d_i are dampened versions of excitations in γ. This behavior can be explained using (4). If a gap is opened by increasing γ the vehicle slows down, this decreases the distance hv_i. Thus, at a time t_1 during a gap opening maneuver starting at time t_0, $\gamma(t_1) - \gamma(t_0) \geq d_{r,i}(t_1) - d_{r,i}(t_0)$. Therefore, d_i may still be changing at the end of the γ-trajectory as the vehicle is still adjusting its velocity. However, a suitable gap is available for the new vehicle when the γ-trajectory ends.

Feedback controller assuming a differentiable γ (FBD) The feedback controller reacts to changes in the error and does not directly use the planned trajectory of γ. In essence, the control law (11) is replaced by

$$\dot{u}_i = \frac{1}{h}\left(\begin{bmatrix} k_\mathrm{p} & k_\mathrm{d} \end{bmatrix} \begin{bmatrix} e_{1,i} \\ e_{2,i} \end{bmatrix} + u_{i-1} - u_i \right). \tag{19}$$

However, $e_{2,i}$ as described by (6) does contain the term $\dot{\gamma}$. It can be obtained by using knowledge of the designed γ trajectory or through an observer. Using the states of (13) the state dynamics can then be written as

$$\dot{x} = \begin{bmatrix} 0 & -1 & -h & 0 & -1 & 0 \\ 0 & 0 & 1 & 0 & 0 & 0 \\ 0 & 0 & -\frac{1}{\tau} & \frac{1}{\tau} & 0 & 0 \\ \frac{k_p}{h} & -\frac{k_d}{h} & -k_d & -\frac{1}{h} & -\frac{k_d}{h} & 0 \\ 0 & 0 & 0 & 0 & 0 & 1 \\ 0 & 0 & 0 & 0 & 0 & 0 \end{bmatrix} x + \begin{bmatrix} 0 \\ 0 \\ 0 \\ 0 \\ 0 \\ 1 \end{bmatrix} \dddot{\gamma}. \tag{20}$$

Using these equations and (16), the transfer function between γ and e_i is found to be

$$\frac{e_i(s)}{\gamma(s)} = s^3 \frac{e_i(s)}{\dddot{\gamma}(s)} = -\frac{s^2 + \tau s^3}{k_p + k_d s + s^2 + \tau s^3}. \tag{21}$$

At low frequencies this transfer function has a small gain, the gain will go to 1 at high frequencies. In essence, at low frequencies the γ-trajectory can be followed closely and thus the error remains close to 0. At high frequencies the γ-trajectory cannot be followed and thus the error has the same amplitude as the γ. The exact behavior is dependent on the system parameters. This behavior is confirmed by investigating the transfer function

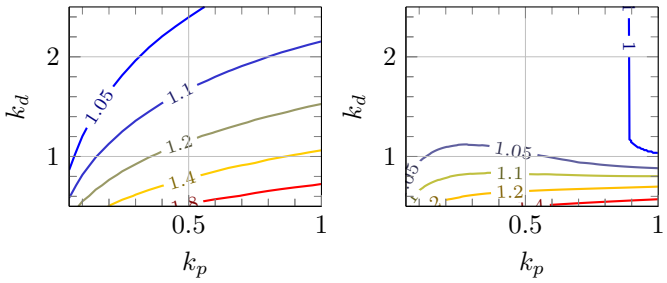

(a) Headway $h = 0.5$ seconds. (b) Headway $h = 1.5$ seconds.

Fig. 2. $\sup_{\omega \in \mathbb{R}} |G_{FBD}(j\omega)|$ with $\tau = 0.1$ for different values of k_p, k_d and h.

$$G_{FBD}(s) = \frac{d_i(s)}{\gamma(s)} = \frac{k_p + k_d s}{k_p + k_d s + s^2 + \tau s^3} \frac{1}{1+hs}. \tag{22}$$

The gain of this transfer function is close to 1 at low frequencies and goes to 0 at high frequencies. Thus, the additional inter-vehicle distance is approximately equal to γ at low frequencies. At high frequencies this distance will be close to 0. The maximum gain of this transfer function is dependent on parameters k_p, k_d, h and τ. In the controller design, parameters k_p, k_d and h can be tuned. However, τ is a system property and cannot be adjusted. For this reason, the influence of k_p, k_d and h have been analyzed for a given τ. The results of the analysis are shown in Figure 2. The maximum gain for some parameter sets is greater than 1. Therefore, γ-trajectories may be amplified in the d_i signal. For a large headway time the maximum gain decreases and may even go to 1. However, the headway time can be constrained by other factors and this solution may thus be infeasible.

Feedback controller assuming a constant γ (FBC) Without knowledge of $\dot{\gamma}$, the feedback control law of (19) can be combined with the error definition

$$e_{2,i} = v_{i-1} - v_i - h a_i. \tag{23}$$

The system with this controller can be written in the form

$$\dot{x} = \begin{bmatrix} 0 & -1 & -h & 0 & -1 & 0 \\ 0 & 0 & 1 & 0 & 0 & 0 \\ 0 & 0 & -\frac{1}{\tau} & \frac{1}{\tau} & 0 & 0 \\ \frac{k_p}{h} & -\frac{k_d}{h} & -k_d & -\frac{1}{h} & 0 & 0 \\ 0 & 0 & 0 & 0 & 0 & 1 \\ 0 & 0 & 0 & 0 & 0 & 0 \end{bmatrix} x + \begin{bmatrix} 0 \\ 0 \\ 0 \\ 0 \\ 0 \\ 1 \end{bmatrix} \dddot{\gamma}. \tag{24}$$

Using this system, the transfer function between e_i and γ is found to be

$$\frac{e_i(s)}{\gamma(s)} = s^3 \frac{e_i(s)}{\dddot{\gamma}(s)} = -\frac{k_d s + s^2 + \tau s^3}{k_p + k_d s + s^2 + \tau s^3}. \tag{25}$$

This equation is similar to (21) with an additional $k_d s$ term in the numerator. The general behavior is thus similar, this is confirmed by the transfer function

$$G_{FBC}(s) = \frac{d_i(s)}{\gamma(s)} = \frac{k_p}{k_p + k_d s + s^2 + \tau s^3} \frac{1}{1+hs} \tag{26}$$

which is comparable to (22). The difference becomes apparent when analyzing the maximum gain. The analysis for this system is shown in Figure 3. A maximum gain of 1 is obtainable with a larger parameter set using this controller. Since $\dot{\gamma}$ is ignored the γ-trajectory is followed less aggressively. Thus, an overshoot in distance less probable.

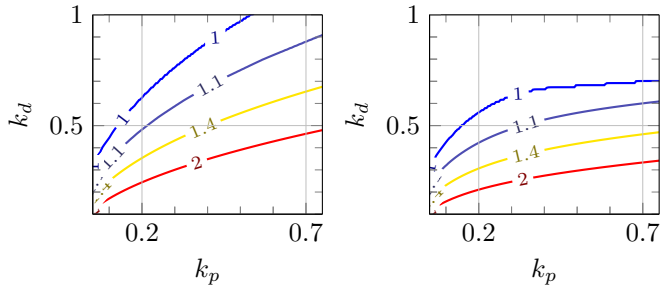

(a) Headway $h = 0.5$ seconds. (b) Headway $h = 1.5$ seconds.

Fig. 3. $\sup_{\omega\in\mathbb{R}} |G_{FBC}(j\omega)|$ with $\tau = 0.1$ for different values of k_p, k_d and h.

2.3 Transient Behavior

For a timely execution of the gap opening maneuver, the transient behavior of the controllers is investigated. First, the impulse response of the *FF* algorithm is analyzed using (18). This transfer function can be written as

$$\dot{x} = \begin{bmatrix} -1 \\ h \end{bmatrix} x + [1]\, u, \quad y = \begin{bmatrix} 1 \\ h \end{bmatrix} x. \tag{27}$$

Using the standard A, B, and C matrix notation in this model, the impulse response $g(t)$ can be computed as

$$g(t) = Ce^{At}B = \frac{e^{\frac{-t}{h}}}{h}. \tag{28}$$

The impulse response shows how the vehicle will return to a constant velocity v_{i-1} after the maneuver. Furthermore, it is apparent that this return is dependent on headway time h. Since $g(t) > 0\ \forall\ t \in \mathbb{R}$ no overshoot of the desired gap is expected.

A similar analysis is performed for the *FBD* and *FBC* controllers using (22) and (26) respectively. Their impulse response is dependent on parameters k_p, k_d, τ and h. Therefore, a numerical example is used for this investigation, where $k_p = 0.2$, $k_d = 0.7$, $\tau = 0.1$ s and $h = 0.5$ s.

The corresponding A-matrix is equal for the *FBD* and *FBC*, in this numeric example its eigenvalues have strictly negative real parts. Therefore, the impulse response of (28) can be bounded as

$$\|g(t)\| \leq ce^{-\lambda t}. \tag{29}$$

All eigenvalues of A have multiplicity equal to 1. Thus λ can be chosen as the absolute value of the largest real part of the eigenvalues of A (Hespanha (2009)). The chosen value of λ is 0.3660, the value of c is estimated numerically to be 0.9842 and 0.9464 for the *FBD* and *FBC* respectively. The resulting impulse responses of all controllers using the previously mentioned parameters can be found in Figure 4.

The impulse response of the *FF* is largest at $t = 0$, since the system reacts directly to changes in γ. Furthermore, there is no overshoot in d_i, since $g(t) > 0$ is satisfied. The impulse response of *FBD* has a larger overshoot than that of *FBC*. The bound on the impulse response for *FBC* is slightly stricter than that of *FBD*. A comparison using a time simulation is provided at the end of this section to highlight the difference in behavior.

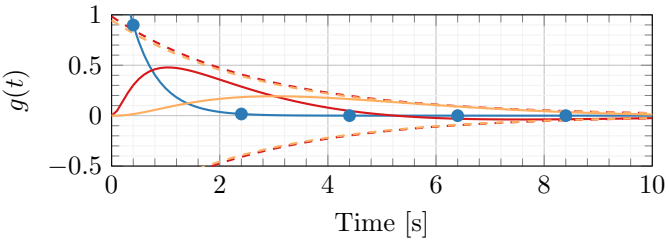

Fig. 4. The $\frac{d_i}{\gamma}$ impulse response of the *FF* (—●—), *FBD* (——) and *FBC* (——), and the corresponding bounds for the *FBD* (- - -) and *FBC* (- - -).

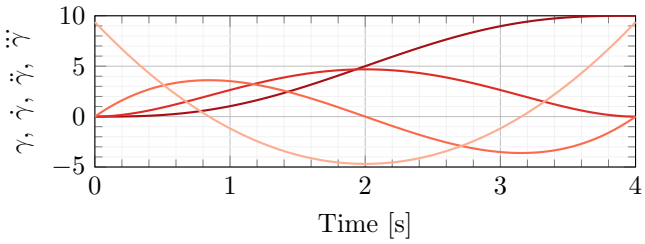

Fig. 5. Example γ-trajectories from 0 to 10 meters in 4 seconds and their derivatives. With γ [m] (——), $\dot{\gamma}$ [m/s] (——), $\ddot{\gamma}$ [m/s^2] (——), and $\dddot{\gamma}$ [m/s^3] (——).

2.4 Trajectory Design

One way to obtain a smooth trajectory that satisfies constraints on the derivatives is the usage of a polynomial. A fifth order polynomial can be used to describe a C^2 continuous γ-trajectory, such that

$$\gamma(T) = c_1 + c_2 T + c_3 T^2 + c_4 T^3 + c_5 T^4 + c_6 T^5. \tag{30}$$

Where T is the time starting from the initiation of γ. Constants c_1 till c_6 are parameters used to give γ the desired behavior. Primarily, $\gamma(T)$ is designed to reach the gap size γ_{end} at time T_{end}, where T_{end} is the desired timespan of the gap opening maneuver. The trajectory of $\gamma(T)$ is designed such that $\dot{\gamma}(T_{end}) = 0$ and $\ddot{\gamma}(T_{end}) = 0$. Initial values γ_{ini}, $\dot{\gamma}_{ini}$ and $\ddot{\gamma}_{ini}$ are considered such that the trajectory can be redesigned at any time. These conditions are fulfilled by selecting the constants

$$\begin{aligned} c_1 &= \gamma_{ini}, \quad c_2 = \dot{\gamma}_{ini}, \quad c_3 = 0.5\ddot{\gamma}_{ini} \\ c_4 &= \frac{20\,(\gamma_{end} - \gamma_{ini}) - 3T_{end}\,(4\dot{\gamma}_{ini} + T_{end}\ddot{\gamma}_{ini})}{2T_{end}^3} \\ c_5 &= \frac{-30\,(\gamma_{end} - \gamma_{ini}) + T_{end}\,(16\dot{\gamma}_{ini} + 3T_{end}\ddot{\gamma}_{ini})}{2T_{end}^4} \\ c_6 &= \frac{12\,(\gamma_{end} - \gamma_{ini}) - T_{end}\,(6\dot{\gamma}_{ini} + T_{end}\ddot{\gamma}_{ini})}{2T_{end}^5}. \end{aligned} \tag{31}$$

An example γ-trajectory for gap opening is shown in Figure 5. The parameters for the γ-trajectory, such as γ_{end}, in this graph are chosen purely for illustrative reasons and do not bear any significance. Every derivative of γ is a polynomial one order lower than previous derivative.

For parameterization of the γ-trajectory, consider an *ego* vehicle opening the gap behind a preceding (*pre*) vehicle. The γ-trajectory should be such that it can accommodate a *new* vehicle when the *pre* vehicle is at a location $q_{end,pre}$. The time constraint of the γ-trajectory should thus correspond with a spatial constraint using

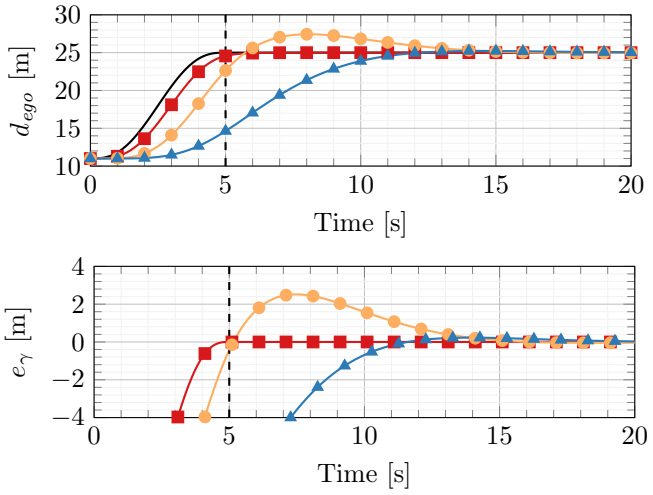

Fig. 6. Simulation results of the gap opening maneuver using three different controllers. With reference $hv_{nom} + r + \gamma$ (——), and the results for the *FF* (—■—), *FBD* (—●—) and *FBC* (—▲—) algorithm, with T_{end} (- - -).

$$\gamma_{end} = h_{new} v_{pre} + L_{new} + r_{new} \tag{32}$$

$$T_{end} = \frac{q_{end,pre} - q_{pre}}{v_{pre}}. \tag{33}$$

Where L_{new} is the length of the new vehicle, and subscripts *pre* and *new* denote the vehicle to which a symbol belongs. It is assumed that the v_{pre} is approximately constant and $v_{new}(T_{end}) = v_{pre}(T_{end})$.

2.5 Simulations

Simulations using this γ-trajectory with the different algorithms are performed using a numerical example. This simulation represents a merging maneuver on a highway on-ramp with a tiny vehicle. Here $v_{pre} = 20$ m/s, $r = r_{ego} = r_{new} = 1$ m, $L_{new} = 3$ m, $h = h_{ego} = h_{new} = 0.5$ s, $\tau = 0.1$ s, $k_p = 0.2$, $k_d = 0.7$ and $T_{end} = 5$ s. The control parameters are taken from Ploeg et al. (2011). Based on v_{pre} and T_{end} there is approximately 100 meters to open the gap. Distance d_{ego} and error $e_\gamma = d_{ego} - v_{ego}h - r - \gamma_{end}$ are shown in the top and bottom graph of Figure 6 respectively. In essence, $e_\gamma = 0$ implies that d_{ego} can accommodate the merge of a *new* vehicle such that $d_i = v_i h + r \; \forall \; i \in \{ego, new\}$. If $e_\gamma < 0$ the gap is too small and if $e_\gamma > 0$ there is additional space. In some literature, the merge is started if $|e_\gamma| \leq \epsilon_d$ where ϵ_d is a predefined threshold (Hult et al. (2018)).

The results using the *FF* control algorithm show that $d_{FF}(T_{end}) < hv_{nom}(T_{end}) + r + \gamma$, and $e_{\gamma,FF}(T_{end}) = 0$. This is because $v_{ego,FF}(T_{end}) < v_{nom}$, the *new* vehicle can thus be accommodated but $d_{ego} < d_{new}$. For a feedback controller, *FBD* algorithm reaches $e_\gamma \geq 0$ earliest. However, it overshoots the desired gap and thus has large excitations. The *FBC* algorithm reaches $e_\gamma \geq 0$ later. The *new* vehicle may thus not be accommodated close to T_{end}. It is therefore concluded that the usage of the *FF* controller is beneficial because it reaches $e_\gamma = 0$ at T_{end} without an overshoot. The benefit of the *FF* controller is especially apparent when threshold ϵ_d is considered in the merging strategy.

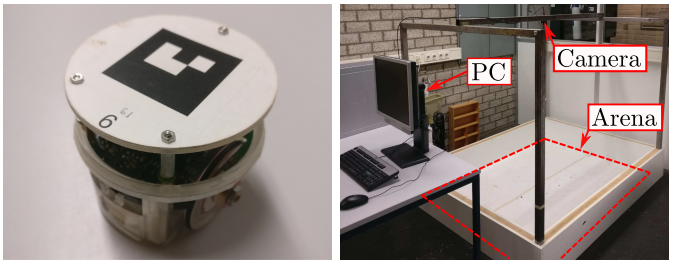

Fig. 7. One of the robots used in this experiment (left) and the arena (right).

3. EXPERIMENTAL SETUP AND RESULTS

3.1 Experimental Setup

Experiments are performed using small differential-wheeled nonholonomic mobile robots (*e-pucks* [1]) in a confined arena. The *e-pucks* were developed by Mondada et al. (2009) and an example is shown in Figure 7. Their left and right wheel are both connected to a stepper motor and can be actuated individually. Their control commands are computed on an external PC and transmitted wirelessly. The PC measures the vehicle poses using a camera above the arena. This localization system uses identifiers on top of the *e-pucks* as developed in Caarls (2009). The arena setup was previously used in Bayuwindra et al. (2020), where a more detailed description of the setup can be found.

Two distinct types of γ-trajectories are investigated. Namely, a polynomial shape described by (30), and a linear shape where γ is not C^2 continuous. The polynomial trajectory is used to illustrate the desired behavior of the controller. It is expected that this controller behaves similarly when any other C^2 continuous trajectory is used. The linear trajectory starts at $\gamma(0) = 0$ and ends at $\gamma(T_{end}) = \gamma_{end}$. $\dot{\gamma}$ is well-defined throughout the trajectory, but $\ddot{\gamma}$ and $\dddot{\gamma}$ are not well-defined at $T = 0$ and $T = T_{end}$. This example of a non C^2 continuous γ-trajectory illustrates the effect on the error dynamics. The *feedforward* (*FF*) and *feedback* (*FB*) control strategies are analyzed. The *FBC* algorithm was used as *feedback* controller.

The proposed gap opening algorithm is intended for automotive applications. Therefore, the control is based on different longitudinal dynamics than those of the *e-pucks*. The velocity of the *e-pucks* can be controlled directly. Thus, the longitudinal dynamics of (2) and (3) are considered in the computation of the control input. In essence, modeled accelerations and driveline dynamics are computed and stored on the PC to obtain the desired velocities.

The vehicles utilize a simple path following algorithm to drive laps around a specified path with a straight. The maneuvers are executed on the straight. Therefore, the lateral dynamics of the *e-puck* are not critical for the accurate modeling of an automotive application. Furthermore, a coordinate transformation is used to measure q_i, v_i, and a_i along the path. Due to this transformation u_i is adjusted. Furthermore, it is considered that the experiments have a centralized control setting. Meaning, a central PC computes the control inputs for all vehicles. However, the intended application of the algorithm is a decentralized

[1] Further information can be found at http://www.e-puck.org.

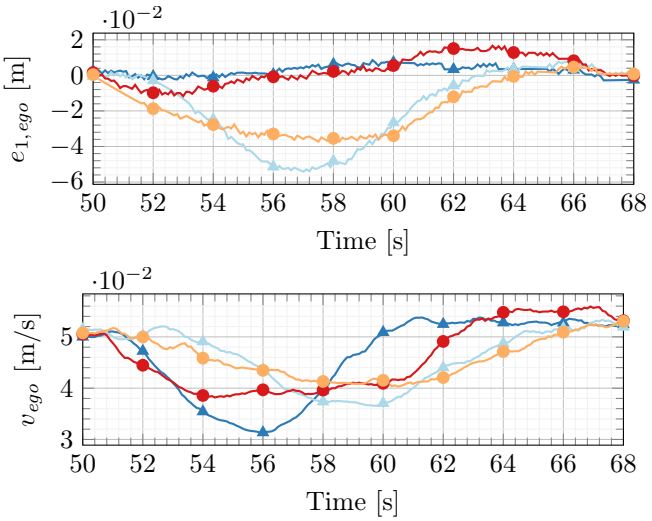

Fig. 8. Error $e_{1,fol}$ for the different γ trajectories during the gap opening maneuvers. For *FF Poly* (—▲—), *FB Poly* (—▲—), *FF Lin* (—●—) and *FB Lin* (—●—).

platoon where each vehicle computes its own control inputs. The available knowledge of the vehicles is considered in the software on the PC. Moreover, communication delays are simulated by holding the control input u_{pre} for one computation step. The system operates at approximately 25 Hz, thus the communication delay is around 0.04 seconds. All experiments were conducted using $\tau = 0.1$ s, $k_p = 0.2$, $k_d = 0.7$ $h = 0.5$ s and $r = 0.1$ m.

3.2 Experimental Results

For spatial or time-restricted merging scenarios, such as highway on-ramps, the timely execution of the gap opening maneuver is the primary objective. Error $e_{1,ego}$ is used as an indicator of the maneuver completion because $e_{1,ego} = 0$ implies $d_{ego} = d_{r,ego}$.

Experiments were conducted for a gap opening maneuver starting at $t = 50$ and ending at $t = 60$. The *pre* vehicle is driving at 0.05 meters per second. Furthermore, γ grows from 0 to 0.1 meters during the maneuver. The algorithms are denoted with *Poly* or *Lin* when a polynomial or linear γ-trajectory is used respectively.

Figure 8 shows the error during the gap opening maneuver. The error when using the *FF Poly* algorithm remained close to 0. The *FF Lin* strategy introduces errors at $t = 50$ and $t = 60$, because $\ddot{\gamma}$ and $\dddot{\gamma}$ are not determined. However, the error goes to 0 when $\ddot{\gamma} = 0$ and $\dddot{\gamma} = 0$. It is shown that at $t = 60$ the position error is zero but the velocity differs from the preceding vehicle. The *FB* control algorithms caused larger errors.

When error $e_{1,ego} \neq 0$ it is implied that the inter-vehicle gap is not the correct size. Therefore, only the *FF Poly* strategy has a timely maneuver execution. The other strategies do not satisfy the objective as the maneuver ends at approximately 67 seconds. Thus there is no significant difference in timeliness of these algorithms. In the context of a merge maneuver this means that only the *FF Poly* strategy would result in a gap with the correct size at the predefined time. This is important to satisfy the spatial constraints of a highway on-ramp environment.

4. CONCLUSION

Research on merging of CAVs does not often consider CACC platoons. In prior research the merging strategies for CACC platoons generally used heuristic methods for the vehicle alignment. However, there is no focus on the fulfillment of time and spatial restrictions. In the current work we aimed to start the development of a cooperative platoon-based merging strategy by tackling the problem of gap opening. The main objective was to execute the maneuver in a predefined time. Experimental validation is performed with small mobile robots.

A gap opening strategy was developed to merge maneuvers with spatial constraints, such as highway on-ramp scenarios. A corresponding controller was designed to ensure the gap is opened in a predefined time. In future work, the desired trajectory of the gap may be optimized. Furthermore, these results can be used in the design of a merging algorithm specifically for CACC platoons.

REFERENCES

Bayuwindra, A., Ploeg, J., Lefeber, E., and Nijmeijer, H. (2020). Combined longitudinal and lateral control of car-like vehicle platooning with extended look-ahead. *IEEE Transactions on Control Systems Technology*, 28(3), 790–803.

Caarls, J. (2009). *Pose estimation for mobile devices and augmented reality.* PhD thesis, Delft University of Technology, the Netherlands.

Hespanha, J.P. (2009). *Linear systems theory.* Princeton university press.

Hult, R., Sancar, F.E., Jalalmaab, M., Vijayan, A., Severinson, A., Di Vaio, M., Falcone, P., Fidan, B., and Santini, S. (2018). Design and experimental validation of a cooperative driving control architecture for the grand cooperative driving challenge 2016. *IEEE Transactions on Intelligent Transportation Systems*, 19(4), 1290–1301.

Mondada, F., Bonani, M., Raemy, X., Pugh, J., Cianci, C., Klaptocz, A., Magnenat, S., Zufferey, J.C., Floreano, D., and Martinoli, A. (2009). The e-puck, a robot designed for education in engineering. In *Proceedings of the 9th conference on autonomous robot systems and competitions*, volume 1, 59–65. IPCB: Instituto Politécnico de Castelo Branco.

Ntousakis, I.A., Nikolos, I.K., and Papageorgiou, M. (2016). Optimal vehicle trajectory planning in the context of cooperative merging on highways. *Transportation research part C: emerging technologies*, 71, 464–488.

Ploeg, J., Scheepers, B.T., van Nunen, E., van de Wouw, N., and Nijmeijer, H. (2011). Design and experimental evaluation of cooperative adaptive cruise control. In *2011 14th International IEEE Conference on Intelligent Transportation Systems (ITSC)*, 260–265. IEEE.

Rios-Torres, J. and Malikopoulos, A.A. (2016). A survey on the coordination of connected and automated vehicles at intersections and merging at highway on-ramps. *IEEE Transactions on Intelligent Transportation Systems*, 18(5), 1066–1077.

Wang, Z., Wu, G., Hao, P., Boriboonsomsin, K., and Barth, M. (2017). Developing a platoon-wide eco-cooperative adaptive cruise control (cacc) system. In *2017 IEEE Intelligent Vehicles Symposium (IV)*, 1256–1261. IEEE.